

CURRENT GRID GENERATION STRATEGIES AND FUTURE REQUIREMENTS IN HYPERSONIC VEHICLE DESIGN, ANALYSIS AND TESTING

Periklis Papadopoulos, Ethiraj Venkatapathy, Dinesh Prabhu
Thermosciences Institute, Moffett Field CA 94035

Mark P. Loomis and Dave Olynick
NASA Ames Research Center, Moffett Field CA 94035

ABSTRACT

Recent advances in computational power enable computational fluid dynamic modeling of increasingly complex configurations. A review of grid generation methodologies implemented in support of the computational work performed for the X-38 and X-33 are presented. In strategizing topological constructs and blocking structures factors considered are the geometric configuration, optimal grid size, numerical algorithms, accuracy requirements, physics of the problem at hand, computational expense, and the available computer hardware. Also addressed are grid refinement strategies, the effects of wall spacing, and convergence. The significance of grid is demonstrated through a comparison of computational and experimental results of the aeroheating environment experienced by the X-38 vehicle. Special topics on grid generation strategies are also addressed to model control surface deflections, and material mapping.

INTRODUCTION

Computational Fluid Dynamics (CFD) is becoming a mature discipline, especially for hypersonic applications. CFD is no longer only an analysis tool but is ready to be used in all stages of design. A number of developments have contributed to this situation. The increased robustness of the CFD codes, along with the low computing cost, the ever-reducing elapsed time to compute (due to improved hardware/memory/CPU speeds), improvements in grid-generation solvers and practices, and user-friendly post-processing tools have all contributed to the use of CFD for design.

Our participation in the hypersonic vehicle design and development has been focused towards "Fast Track" NASA programs that employ concurrent engineering as the project philosophy. Current missions employ the concept that the cycle of the vehicle's design to first flight is to be achieved in 2-4 years which dictates a short design cycle with concurrent engineering and manufacturing. This concurrent engineering approach requires high-fidelity solutions from the very beginning. As the design details evolve, the analysis must be able to quickly mature the design. This new reality of schedule, cost and accuracy (in that order of priority) has required us to rethink the process. Introducing CFD analysis in the very early design phase in such an environment has been a great challenge, and has required us to look at the overall process of providing low cost, high-fidelity CFD solutions in a reasonable time. One of the most important elements that required special attention is the grid-generation process. The grid-generation process needs to be very efficient, adaptable, cheap, fast, flexible, and user friendly. Complex configurations and the important physical phenomena are two aspects that can rapidly change during the early design process. We illustrate this through many examples in which CFD is applied from the very beginning of the concept through design, development and testing.

Our involvement in the hypersonic vehicle design is to provide external aerodynamic and aerothermodynamic environments. The requirements for grid generation are determined from the simulation objectives. Aerodynamic simulations are required to determine the stability and controllability

of the design and to provide loads for the internal structural design. The CFD simulations focused towards aerodynamic environments can also provide integrated forces and moments, surface pressure and shear-stress. Aerothermal simulations are performed to design the necessary Thermal Protection System (TPS) and this focus requires higher fidelity than the aerodynamic simulations. The combined aerothermodynamic environment simulations provide heat-flux, wall temperature, species distribution in the boundary layer, boundary-layer thickness, "real-gas" effect such as catalytic component of the heating, surface streamlines, etc. Determining the appropriate requirements for the grid generation process is complex, difficult to quantify, and most often requires experience. The "art" of grid generation, if not understood and practiced well, can result in significant program impact. The intent of this paper is to present our grid-generation practices, demonstrate the choices and selection reasons and demonstrate the complex issues that limit our grid-generation ability. Finally, suggestions are made to the grid-generation community to develop better, faster and cheaper ways of generating high quality grids to meet our future needs.

The general requirements for grid generation for hypersonic vehicle design, analysis and testing are discussed. Both the geometric complexity and the flow-physics complexity dictate the effort and time required to generate a single initial grid. Some grid-generation approaches may be better than others, when generating a single grid under one set of conditions. The same methodology may not be as efficient when it comes to generating many different grids. The accuracy/fidelity and the cost of the solutions are determined not only by the grid generation approach/philosophy, but also by the type of solver and the computer requirements. Though it is possible to compare the impact of one grid generation approach versus another, the tactics we have adopted is to ask how soon we have to produce the CFD simulation at various stages of design, development and testing. Then, we determine the grid generation requirements through the quality and quantity of grids needed to provide sufficient fidelity solutions in a timely manner to impact the design.

The early design process can extend anywhere between 2 months to 6 months. In the past, experience, coupled with simpler engineering methodologies and/or fast wind-tunnel simulations, have been used in this stage of design and they will continue to be used. On limited occasions, CFD simulations have been needed due to lack of engineering data. The factors that limit the use of CFD in the early design phase are how quickly the grids can be generated and how quickly "sufficiently" accurate CFD simulations can be provided. For complex shapes, 10 – 100 CFD solutions with marginal fidelity but a very fast turn around time, would allow CFD to be part of this stage.

As the design matures from the concept stage to a complete configuration evaluation, operational capability of the integrated design is needed to determine whether the design can meet the mission objective. In addition, in this design stage, the environment for the detailed design of sub-systems and components are needed as well. The geometry in a global sense is well defined, but the operating environment and the design details are not. The design evaluation requires large number of higher-fidelity simulations and CFD can and has played a significant role. A large number of global simulations for a range of operating conditions and evaluation of design details for the complex operation space may be required. The grid generation requirements at this stage are to model the global geometry with the required fidelity, not to include the design details but to provide higher fidelity global solutions through grid-refinement/grid adaptation, compared to the early evaluation phase. The simulations for the design details or local issues, require modeling both simpler and complex local details with adequate accuracy under the environment dictated by the global simulations. This means that the grid-generation process needs to be able to meet the requirements from the above two considerations.

Once the overall design has been achieved and the environment for the local design issues have been determined, the local /sub-system design is further refined along with sub-system and component design qualification through ground-based simulation. Along with the ground-based simulations, CFD simulations are also used at this stage to determine the margins and safety factors. CFD simulations are also validated with ground based simulations to assess their accuracy. On the other hand, CFD is used to extrapolate the ground-based measurements to flight. Through the combination of ground-based testing and CFD simulation and extrapolation to flight, not only the margins, but also the detailed performance capability of

the vehicle is determined to reduce risk. The requirements on CFD and hence on grid generation, at this stage are increased fidelity, as good a simulation as possible, requiring large grids along with grid adaptation/refinement for a few "design-limiting" conditions and ground-based experimental simulations.

In the case of experimental flight test programs, such as X-33 and X-38, CFD is also used in pre-test flight predictions and post-flight analysis and the requirements for CFD and grid generation are a combination of the ones we have outlined above and more. Ultra-fast simulation capabilities, if available, can be used, not only to select the most appropriate trajectory, but also post-flight analysis can be performed as soon as the flight data is made available. For concepts such as Reusable Launch Vehicle of the future, "smart and fast" CFD simulations can play a significant role. The above-mentioned details are provided here not only to stress the importance of grid generation, but also to emphasize the fact that program requirements from top down determine the grid generation requirements.

Grid generation remains one of the most time consuming aspects of numerical simulations of complex configurations. This is especially true in CFD and its integration in vehicle design. The methodologies and strategies implemented in support of the X-33 hypersonic vehicle CFD analysis and the X-38 Experimental Crew Return Vehicle are presented in this paper. This paper will also address special topics on the topological construct for flap deflections, gaps, material mapping, and the vehicle afterbody. The physics of the problem at hand must guide the grid-point distribution in computational space to represent the physical solution with sufficient accuracy. The paper will also address grid refinement strategies, the effects of wall spacing, and convergence studies. The significance of grid quality to accurately capture the physical phenomena is demonstrated through a comparison of computational and experimental results of the aeroheating environment experienced by the X-38 vehicle.

GRID GENERATION CODES AND ASSOCIATED TOOLS

For the applications described in this report, the surface and volume grid generations required the use of a number of grid generation codes. A combination of these codes was used to address specific grid-generation applications. The adopted CFD hypersonic reacting-flow code (GASP), handles structured, single- or multi-zonal grids. For hypersonic ideal gas computations the OverFlow code and the Chimera tools are implemented. It should be noted that these codes frequently constrain the use of specific grid generation techniques. The description of the employed grid-generation codes and tools is presented here.

GridGen

GridGen is a commercially available 3-D grid generation program.¹ It is a tool for developing multi-block structures, inter-block connections, and surface and volume grids. The following four data entities are available in GridGen for use during construction of a volume grid: (a) databases, (b) connectors, (c) domains, and (d) blocks. A database is an input that provides the geometric definition of the object for which the grid is constructed. Database files are imported from computer-aided-design codes. Gridgen also has built-in database manipulation capabilities. Connectors are user-generated curves on which grid points are distributed. A number of elemental curve segments are available in GridGen such as poly-lines, poly-curves, conics and circles that can be combined to compose the desired shape. Domains (or surface grids) are generated by grouping the connector lines to define the domain perimeter. The interior grid domain is automatically constructed using either an algebraic method called transfinite interpolation or an elliptic partial-differential equation method to improve the distribution of surface grid points. Finally, blocks (or volume grids) are assembled by selecting the six sides (domains) of the volume. An elliptic partial differential equation method can be implemented to improve the final distribution of volume grid points.

HypGen

The HypGen program² originally developed by Steger and Ritk³ is a hyperbolic, 3-D, grid generator. It requires a single-block surface grid input. Other input parameters include variable far-field definition and initial/end grid spacing and a stretching function. The 3-D hyperbolic grid generation equations are solved by using two orthogonality relations and one cell volume constraint. The volume grid is generated marching away from the user-supplied surface grid with a step size given by the stretching function in the normal direction. HypGen can be run through a graphical user interface or in a batch mode. It also provides visualization hooks to PLOT3D⁴.

HyperMesh

HyperMesh⁵ is a commercially-developed finite element pre- and post- processor that quickly creates finite element and finite difference models for engineering analysis. HyperMesh uses the following building process: (i) import and translate surface geometry from an external file, (ii) create collectors and components, (iii) build the model by building elements, (iv) mesh the model and (V) check the mesh quality. It also provides for extensive CAD surface manipulations. Of particular interest is the ability of HyperMesh to do automatic mesh generation and surface stitching. The organization of the mesh generation module focuses on providing tools that supply automated assistance. A number of mesh-generation algorithms, algorithm parameters and smoothing operations are available to improve grid quality. The available mesh generation algorithms are divided into two types: those that require the presence of a surface and those working purely from node or line data. The smoothing algorithms are categorized as size or shape corrected algorithms. The size correcting smoothing uses a modified Laplacian over-relaxation. The shape correcting smoothing algorithm employs isoparametric-centroidal over-relaxation that corrects the elements' shape allowing variation in element size.

GridPro

GridPro⁶ is a commercially available 3-D, multi-block grid generator. The philosophy of GridPro is to minimize user input and provide many automatic features. For the applications presented in the paper, the code demonstrated optimal grid distribution. An advanced smoothing scheme is utilized to provide high grid quality. Grid generation is performed by solving a variationally-based method with an iterative updating scheme. This method is more computationally intensive and requires multiple sweeps to generate a grid as compared to an algebraic grid-generation algorithm. The increased computational effort is the result of the philosophy of minimizing user input and is needed to generate grids of superb quality. The improved grid quality results in faster flow convergence of the flow solvers, and higher flow-solution accuracy. The increased convergence also reduces the computational expense. The grid-generation methodology requires three steps. First, the surfaces that define the computational volume are imported and specified. Surfaces are either imported from a CAD program or generated within GridPro. A number of surface generation utilities and tools are available. Next, the general topology is constructed using available tools. Corner points are assigned to the appropriate surfaces. Grid density assignments are made for the current topology. A topology input language is used to record the topology into a file. Lastly, the volume grid is computed and processed for quality check. The quality-check information includes warpage statistics and the upper and lower bound fold counts. Block connectivity information is automatically stored in a file. The computed grid is not clustered at the walls and is suitable only for inviscid simulations. Four options are available for algebraic clustering to surfaces. A number of utilities and tools are provided to display, analyze, extract, convert, print and weld data or grids.

SAGE

SAGE is a multidimensional self-adaptive grid code. The basic formulation follows the method of Nakahashi and Deiwert⁷. Many recent modifications have been made to facilitate the use of SAGE⁸ for complex three-dimensional grid adaptation and restructuring. Local truncation errors are minimized by adapting grid points in regions of strong gradients. This approach results in enhanced flow-field resolution. The methodology implemented in SAGE reduces complex three dimensional grid adaptation to a series of one dimensional problems along the computational grid lines. The approach taken is to implement tension

and torsion-like spring forces proportional to the local flow gradient. Tension forces control the clustering of points to strong gradient regions, while torsion forces maintain smoothness and orthogonality between adjacent grid lines. A triadiagonal solver provides the location of grid points by finding the new equilibrium position of the computational grid. In hypersonic vehicle simulations, the computational boundaries are initially over- or under-estimated, thus resulting in lack or excess of sufficient grid points. Non-equilibrium reacting flows are computationally intensive. It is therefore important to determine the minimum grid requirements to provide high fidelity surface heating at the vehicle's surface. For this purpose SAGE was used to move the grid's outer boundary and fit the computed shock envelope location. The interior points are then redistributed along the computational grid lines normal to the vehicle's surface. A number of outer boundary movement and wall clustering options are available. SAGE is extensively used to modify space vehicle volume grids when CFD is performed for a wide range of angles of attack and flight conditions for the same vehicle configuration. Two re-clustering options are available in SAGE. The first option results in redistribution of points proportional to the original grid point distribution. The second algorithm⁹ results in a hyperbolic distribution based on user-supplied first and last grid spacing. Two additional utilities are available within SAGE for outer surface smoothing and smooth transition at the boundary layer edge.

MASTERMINDING, CONCEPTUALIZING AND DESIGNING GRIDS

Advanced planning and strategizing is important before any grid generation activity is initiated. Careful planning, targeting and evaluation of the key steps required to meet the desired grid quality can minimize the time for mesh generation with maximum solution accuracy along with total cost, time and labor minimized. Strategizing includes recognizing the grid requirements to appropriately model the physical phenomena and evaluating the available grid generation/modification tools to meet the outlined milestones. It is important to design and evaluate the topology first in areas of geometric complexity, such as wings, fins, flaps, gaps, penetrations, etc. In most vehicle configurations the geometric complexity is towards the aft end. The general topology constructed in regions of geometric complexity dictates the guidelines for designing the topology toward the nose of the vehicle. In addition, to take advantage of sequencing to accelerate the flow solver convergence, the grid should be designed to preserve the geometric integrity of the vehicle at coarser grid-sequence levels. Intermediate regions between corners and sharp edges should be sequencable to the same grid coarseness level as the overall master grid. In addition to accelerated convergence, grid sequencing is also used to establish a grid independent CFD solution (or minimize grid dependency and maximize solution accuracy). Grid sequencing is done progressively in the directions where strong gradients dominate. Grid point distribution and density must be selected to meet the grid sequencing requirements. Other factors considered in designing grids include the optimal grid size, the choice of the numerical algorithm to be used in the CFD solver, accuracy requirements, computational expense, and the available computer hardware. The methodology adopted and the combination of grid generation tools selected should account for possible vehicle configuration changes and grid modifications from the very beginning.

VEHICLE SURFACE (OUTER MOLD LINE) REPRESENTATION

The first step in any grid generation process is the surface definition. One of the most critical obstacles in sharing data between CAD, grid generators, CFD and visualization codes is data formats. For CFD to contribute to design, the cycle time from CAD to CFD needs to be reduced during the initial design stages when the geometry is changing frequently. Currently, significant time and effort is spent in data conversion throughout the exchange process. Future grid generation codes should streamline this process and make it transparent to the user. In most cases, grid generation starts from a CAD model. CAD models are typically generated for design applications and are generally not suited for grid generation. A "water tight" outer mold line (OML) definition is needed for grid generation. Reparation of surface integrity, closure of gaps, removal of overlap, modification of difficult to mesh regions, and organization and elimination of excess elements are normally required before the mesh generation process is initiated. In

addition, surface repair tools may be used to simplify geometric complexities, or define volumes for compact grid enrichment where detailed subsystems analysis may be required. The number of possible grid topologies is ultimately related to the vehicle surface definition and complexity. As the vehicle design matures, configurational changes are more localized. The surface definition for detailed analysis needs to be parameterized and linked to high fidelity grids for local flow studies.

GRID GENERATION METHODOLOGIES

Generation of computational meshes around a 3-D configuration is another bottle-neck in the application of CFD to complex configurations. A number of grid generation codes were employed to develop methodologies and streamline the grid generation process with the ultimate goal to substantially reduce the manpower and time required to build high quality grids. Expertise was developed in the use of hyperbolic, elliptic, algebraic, grid adaptation and modification tools. Specifically, a combination of HypGen, Gridgen, GridPro and SAGE codes was used to develop strategies and grid generation methodologies.

Most of the grid generation methodologies implemented in support of the X-38 CFD work to define the hypersonic aerothermal environment used a combination of GridGen and HypGen. GridGen was mostly used for surface grid generation and HypGen was found to be more efficient for the volume grid generation. Especially near the vehicle's surface HypGen produced grids of high quality for complex geometries. Grid orthogonality near the vehicle wall was important for resolving the viscous and thermal layers. The shortcomings of HypGen were in the specification of the outflow boundary. The methodology implemented was to initially generate a volume grid that encloses all possible shock envelope locations for all the angle of attack cases and flight conditions along the flight trajectory considered. The code SAGE, was then applied to re-cluster grid points along the grid lines normal to the surface and relocate the outer boundary of the volume to fit the shock envelope for each flight condition case.

For problems of geometric complexity, HypGen was used to construct the grid near the vehicle surface enclosing the boundary layer where grid orthogonality was important. GridGen was then used to fill the rest of the volume grid using transfinite interpolation techniques. Finally, SAGE was applied to match the grid spacings and smoothen the transition between the viscous HypGen and inviscid GridGen volume grids.

For the X-33 program the GridPro code was used to reduce grid generation time, improve grid quality and automate volume grid modifications. This code provides a different approach to grid generation. Grid generation using GridPro requires three distinct steps: (A) provide the surfaces that enclose the volume where the grid is to be generated, (B) build the grid topology, and (C) assign topology corner points to the appropriate surfaces. The grid generated is uniformly distributed in the normal direction to the vehicle surface. A set of utilities is supplied for clustering grid points near the vehicle's surface. This methodology is very advantageous because volume grids can be generated automatically when the vehicle surface or the angle of attack are modified since the general topology (item A) and its assignments (item C) remain the same. This approach is directly in line with the ultimate objective to automate grid generation and improve grid quality.

GRID QUALITY AND VALIDATION

The next step in the process is to ensure grid quality. The accuracy of the computed solution is the ultimate measure of grid quality. Grid refinement studies are required to establish grid sensitivity and criteria for a grid independent solution. Grid quality is dependent on the grid point distribution, grid skewness, cell warpage, cell aspect ratio, smoothness, orthogonality, adaptation to the flow features, numerical algorithm used in the flow solver, and the flow parameters of interest. Finally, to further quantify grid quality it is important to validate the numerical computations at different levels of refinement against available experimental data.

The importance of grid refinement, and the sensitivity of physical models were recognized early in the initial design phases of the RLV-related technology development, both for the X-38 and X-33 programs. Grid generation and computational methodologies were studied to establish the grid requirements for accurate aerothermal environment simulations. This evaluation was comprised of code validation studies against experimental data in conjunction with grid resolution comparisons. Wind-tunnel data in the form of surface pressure and heat-transfer rates were used to determine the solution and grid accuracy.

A number of axisymmetric CFD simulation studies of grid refinement, and sensitivity were examined. A goal of the axisymmetric studies was to evaluate the sensitivity of heat-transfer calculations to the grid resolution and convergence. These studies showed that a computational mesh and a level of convergence which results in accurate surface-pressure and shear stress values, do not guarantee accurate heat-transfer values. Predictions of the aerodynamic environment do not require the same level of grid refinement. Using the GASP code, five or more orders of magnitude reduction in the residual were required to achieve accurate steady-state heat-transfer values. The precise value of the residual drop is problem and code dependent. Axisymmetric calculations were also used to show that heat-transfer predictions are sensitive to the flux splitting method and the limiter choice. A grid which is sufficient for the computation of heat transfer with one choice of flux splitting and limiter may not be sufficient with another choice. Two important parameters to monitor during convergence are the cell Reynolds number defined as

$$Re_{cell} = \frac{\rho_{wall} \alpha_{wall} \Delta y}{\mu_{wall}} \quad (1)$$

and the temperature jump from the wall to the first cell center. In Eq. 1, ρ is the density, μ is the viscosity, α is the speed of sound, and Δy is the normal grid spacing at the wall. For a hypersonic vehicle with a grid of fixed spacing at the wall, the temperature jump and cell Reynolds number decrease streamwise since the boundary layer thickness increases. This observation suggests that grid spacing can be relaxed progressively towards the back of the vehicle. A proper grid resolution study which monitors the temperature jump across the first spacing off the wall and cell Reynolds number, should provide the criteria for the optimum first cell spacing for the whole configuration.

It is strongly recommended that grid refinement and validation studies be done first on 2-D, axisymmetric, or simplified 3-D geometries since computations are more economical than full 3-D complex configuration simulations. These results formed the basis of methodologies adapted in the simulations of the X-33 and X-38 vehicle configurations that will be presented later.

X-38 / GRID REFINEMENT, VALIDATION AND PREDICTION

The goal of the X-38 program is to flight test and demonstrate an experimental Crew Return Vehicle (XCRV) capable of returning International Space Station (ISS) crew members safely to Earth in the event of an emergency. The vehicle shape is a derivative of the X-23 and X-24A lifting body configurations which were flown in the late 1960's and early 1970's. The aerodynamic and aerothermodynamic databases for this vehicle relies on X-24 flight data, extensive ground-based hypersonic facilities^{10,11,12} data, and CFD simulations. Real-gas CFD solvers, once properly validated, are used to verify existing data. This section presents the work performed for the X-38 vehicle and the associated grid generation issues and solutions. The CFD simulations had three objectives: 1) establish the accuracy of the predictions, 2) verify the aerodynamic database derived from X-24 and wind-tunnel data for the full scale flight vehicle, and 3) provide high-fidelity aerothermodynamic environment for the heat-shield design. The CFD simulations comprised of wind-tunnel simulations for a scaled model and full-scale predictions on a nominal design trajectory. An extensive number of simulations prior to the validation exercise were carried out to determine the grid sensitivity on solution accuracy.

Grid Generation

X38 - Evaluation of Deflected Flap Grid Topologies

The computational studies performed with GASP to help establish an efficient approach for distributing the mesh points in the X-38 aft region is presented in this section. These studies also allowed preliminary investigation of the importance of the flow under the flap. A 0.2 m flat plate geometry incorporating a 10° flap was chosen for this study and three types of grids were considered. The first grid used a zonal approach (Fig. 1a, and Fig. 2b) with up to five zones. Zones 1 and 2 are rectangular grids over the front of the flat and over the flap region, respectively. Zone 3 is located next to the flap and has a triangular cross section. It collapses into a singular line at the flap hinge. The singular line in zone 3 lies across an area where it may affect the flow between zones 1 and 3. The singular line was modeled within the given options of GASP as a zonal boundary. One cell from the upstream zone mapped into all the cells corresponding to the singular point location in the downstream grid. Zone 4 is located under the flap and is the same shape as zone 3. It is included for simulations of the flow under the flap. The singular line associated with zone 4 is located along the hinge line where there is no flow, so it does not affect the accuracy of the solutions. Zone 5 is rectangular and was added to include the base region. The second grid topology approach (Fig. 1b and Fig. 2a) wraps the mesh lines around the flap. This eliminates the singular line of the first approach. The disadvantage of the second approach is that the surface geometry must be altered to allow the grid to wrap around the flap, i.e. the point where the flap joins the body must be smoothed so that it is no longer a singular point. This approach also increases the number of points in the circumferential direction throughout the grid, making the solution on the upstream portion more costly than it need be. A third approach (Fig. 1c) also uses a wrap-around grid; however, a singular line is introduced to avoid using extra circumferential points in the upstream region. This approach proved to be very unstable for the solver and was not pursued further.

All grids were created with a 1 μm wall grid spacing. Both the wrap-around and zonal grids have viscous stretching along the side wall of the wedge. For the zonal grids, this required the circumferential lines to be clustered in the side-wall region, thus pulling points from elsewhere on the flat plate. This clustering also resulted in unnecessary circumferential points upstream. The surface grid, exit-plane grid, and the zonal and wrap-around topologies are shown in Fig. 2 a,b.

Singular Axis Effects

For cases assuming no flow through the side flap, the surface pressure and heat-transfer rates for the zonal (Fig. 2b) and wrap around (Fig. 2a) grids were compared. Examining the pressure profiles for the zonal topology shows that beginning at the singular-line zonal boundary between zone 1 and zone 3 the pressure increases for no physical reason. An even more significant error is seen in the heat-transfer plots. This non-physical behavior is not observed for the wrap-around grid, which has no singular line. The error in the zonal-grid solution is related to an abrupt change in cell shape (from rectangular to triangular) in the boundary layer and difficulty in achieving the same grid distribution across the zonal interface. There is also some uncertainty in prescribing the GASP zonal boundary conditions for this topology, which may also contribute to the error. Grid-refinement studies show that the errors can be reduced with finer grids but the present case illustrates that care must be taken to avoid errors with this particular zonal approach. Both grid topologies compute a drop in pressure and rise in heat transfer at the edge of the flap and side-wall interface.

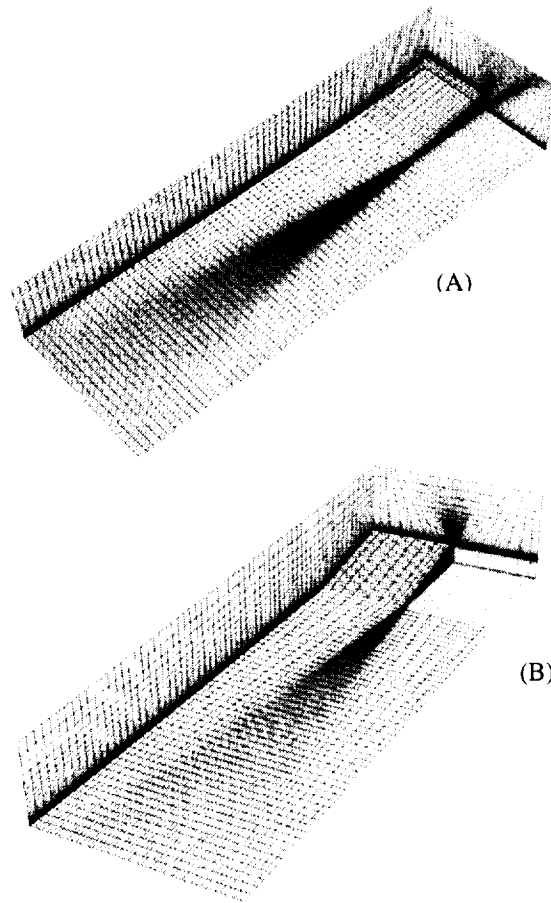


Fig. 2 a,b Grid topologies, (a) zonal, and (b) wrap.

Flow Modeling Under the Flap

The wrap-around grid was used to compare the case where flow is allowed through the flap side wall and under the flap to the baseline case where no flow is allowed under the flap. The results show that there is little influence on the external flow when including the flow under the flap. Note that since reversed subsonic flow was observed beneath the flap, extrapolated boundary conditions are not valid in the exit flow regions. As a result, an additional simulation, which incorporated a base grid, was added to the end of the original computational domain to ensure supersonic flow at the exit plane. This computation resulted in significantly different flow under the flap but again did not change the external flow.

From this study the wrap-around grid approach appears preferable primarily because it avoids the singular lines. With the current GASP options, singular lines, especially those within the boundary layer, cause disruptions in the flow field. The wrap around approach also demonstrated a better convergence rate than the zonal grids with the singular line. A limitation of the wrap-around topology is the difficulty in applying it to even more complicated geometries where a zonal approach would be advantageous. The flexibility of zonal interfaces, which allow for changes in the number of grid points, increases available grid-topology options.

Volume Grid Generation

Grids were generated with the GridGen and HypGen software packages. The nominal grid consisted of 81 points in the streamwise direction, 93 points circumferentially, and 61 points in the normal direction. Care was taken to assure grid orthogonality and smoothness on the surface. An initial solution was obtained on a grid that is much larger than the shock envelope. OutBound was used to adapt and move the outer boundary near the shock and to recluster the body-normal points in the boundary layer. This procedure ensured the efficient use of grid points. In addition, instead of generating grids for each angle of attack separately, the original grid was adapted to each case using SAGE and thereby the time spent to generate grids was reduced significantly.

To establish error metrics and to demonstrate the dependency of the solution quality on the choice and distribution of the grid points and on the numerical solvers, a number of simulations were performed. If the number of grid points in each direction were selected to facilitate mesh sequencing, i.e. at least 3 levels of coarse grids could be constructed easily from the nominal grid, then the CFD simulations could be obtained progressively from the coarser grid. This procedure drastically decreases not only the time to converge the solution on the nominal (finest sequence) grid but also provides a measure of grid independence of the converged solution. The surface grid topology and a surface grid are shown in Fig. 3.

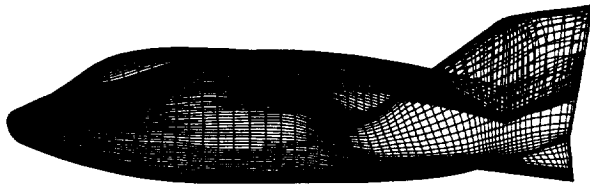


Fig. 3 X-38 Geometry and computational surface grid topology.

Effect of Axial and Circumferential Refinement

The effect of axial and circumferential grids refinement is shown in Fig. 4a, which is a plot of the surface heat flux on a constant circumferential grid line that starts at the nose and passes through the middle of the flap on the windward side. The initial wall spacing is set to 3 microns which corresponds to a maximum wall-cell Reynolds number on the order of 2-3. It is seen that in most areas the coarse-grid (41 x 47 x 61) solution is very close to the finest-grid (161 x 185 x 61) solution. The largest difference occurs in the flap region which consists of a complex separated flow where the effect of local grid is significant. Figure 4b shows the grid refinement effect along a constant axial grid line that runs from the windward to leeward side. Again the sensitivity is small. Assuming that the finest grid provides the most accurate solution, an error estimate is made from the coarser grid solution, shown in Fig. 4c. Based on this estimate, it was decided that a nominal grid of (81 x 93 x 61) was sufficient to resolve the aeroheating in the axial and streamwise directions. However, the (41 x 47 x 61) grid provides a reasonably good prediction and the CPU time required for the (41x47x61) grid is 0.25 of that of the nominal grid.

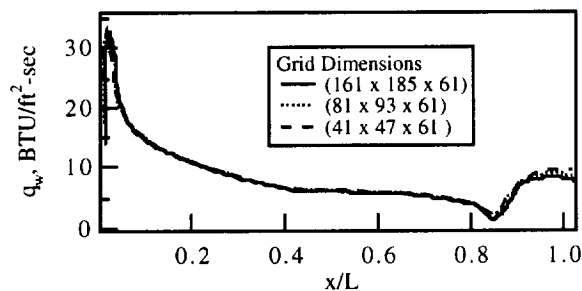


Fig. 4a Effect of axial and circumferential refinement - windward side heat flux.

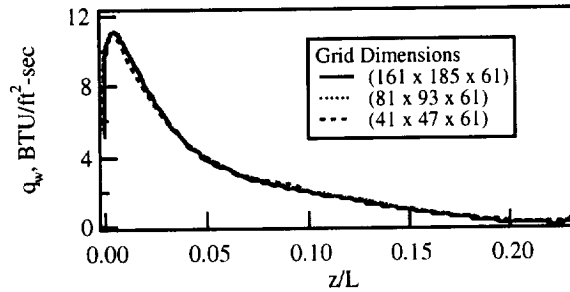


Fig. 4b Effect of axial and circumferential refinement - heat flux along an axial cut ($x/L=0.5$).

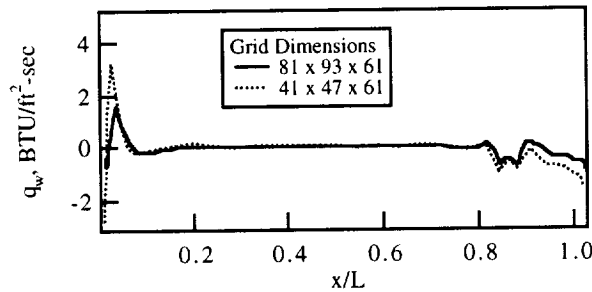


Fig. 4c Error in windward side heat-flux prediction.

Number of Points in the Normal Direction

The number of grid points in the normal direction affect the boundary layer and the wall heat flux significantly. The effect of the number of points in the normal direction is shown in Fig. 5 which is a plot of the windward centerline heat transfer. Cases are run with 31, 51, 61 and 121 points in the normal direction. To save time only the forebody was included in the study. The results show a significant over-prediction of heat transfer with only 31 points, however the grids with 51 or 61 points produce values that are much closer to the 121-point case. The error in heat-transfer prediction between the 61-point grid and the 121-point grid is no more than 1 BTU/ft²-sec and occurs near the singular point at the nose. Based on this study it was decided that 61 points in the normal direction was sufficient.

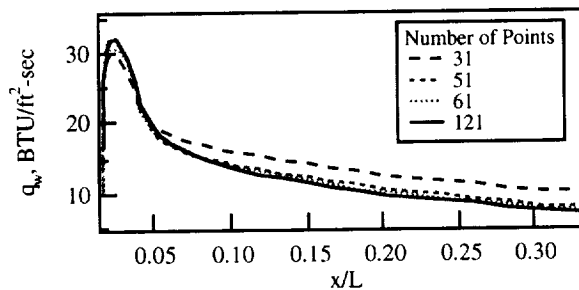


Fig. 5 Grid refinement study, effect of number of points in the normal direction.

Effect of Wall Spacing

In addition to the number of grid points in the normal direction, the distribution and the spacing near the wall affects the wall heat-flux prediction. The effect of initial wall spacing is shown in Fig. 6 for the nominal grid. The nominal grid spacing is 3 microns which corresponds to a maximum cell Reynolds number of about 2-3. The remaining grid points were stretched in the normal direction according to the reclustering algorithm in the SAGE code. It can be seen that the predicted heat transfer changes no more

than 1 BTU/ft²-sec with a factor of three change in cell Reynolds number. However, a large wall spacing, especially at the nose, has the effect of increased heat transfer.

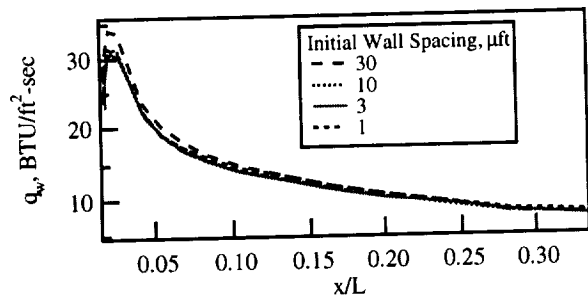
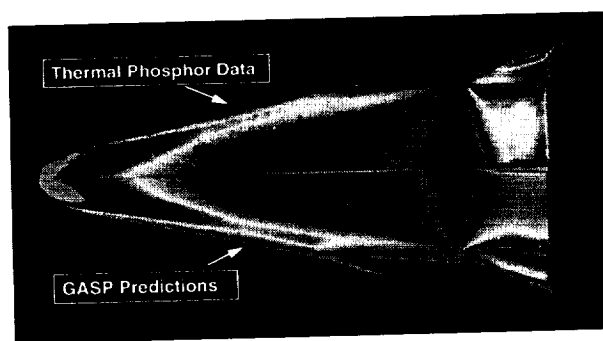


Fig. 6 Effect of wall spacing on heat transfer.

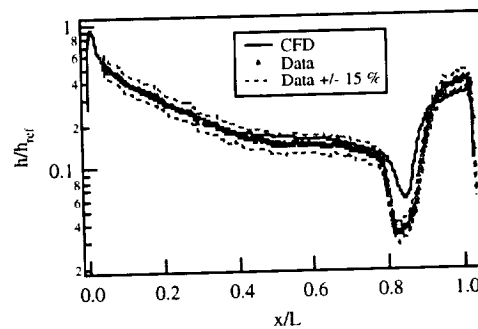
Thus, a wall spacing with a cell Reynolds number no greater than 5, combined with smooth stretching from the wall to the shock with 61 grid points, is able to provide sufficient solution accuracy.

Comparison with Aeroheating Data

To validate the aeroheating predictions, computational simulations are compared with the heating data derived from the thermographic phosphor technique^{13,14} in the NASA Langley 31-Inch Mach 10 facility. One set of flight conditions selected for comparison is shown here. The case is representative of the angle of attack, body-flap setting, and Reynolds number expected during entry. Fig. 7 shows a comparison of the experimental and numerical results. Fig. 7a depicts global values of the non-dimensionalized heat transfer coefficient h/h_{ref} . The comparison shows the features and trends observed in the experimental image to be captured well by the computational simulation. The only visible discrepancy between the data and the CFD is in the flap region, where the CFD is slightly lower. It was assumed that the flow was laminar in the reattachment region at the Reynolds number of this test. If the flow is transitional or turbulent the heating would be higher. The longitudinal comparison of h/h_{ref} at a station slightly off from the bi-symmetry plane is shown in Fig. 7b. The overall agreement is generally within the experimental uncertainty, estimated to be around $\pm 15\%$. Additional details and comparisons, are presented in Ref. 15.



(A)



(B)

Fig. 7 Comparison of experimental and computational results, (a) global values, (b) longitudinal cut.

Flight Cases

The X-38 atmospheric entry trajectory is shown in Fig. 8. The entry duration is about 1600 seconds, with an 800-second period of nearly uniform heat flux. Stagnation-point heat transfer to a 1-foot diameter, cold wall reference sphere calculated using the Fay-Riddell method is also shown.

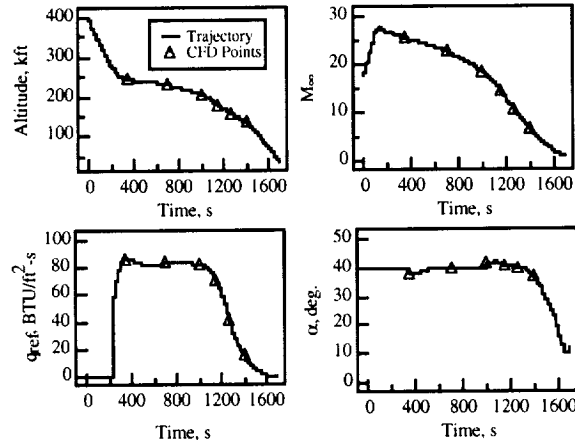


Fig. 8 Time histories of altitude, Mach number, reference heating rate, and angle of attack for the flight trajectory.

Five points from the trajectory profile are initially chosen for calculations. The cases are all run at an angle of attack of 40° and a body flap setting of 25° . The results of the Mach 25.5 case with the fully-catalytic wall boundary condition (i.e., the atomic oxygen and nitrogen species in the shock layer recombine completely at the wall to give molecular oxygen and nitrogen, respectively) are shown in Fig. 9. The grid is clustered near the wall, with a wall spacing of 10 microns at the nose and 30 microns near the tail. This was found to produce a temperature jump on the order of 20°R which is considered sufficient for a grid independent solution. The level of heat transfer during the peak-heating phase is near the maximum allowable for single-use, high-density TUF-coated space shuttle tiles. The CFD simulations predicted wall temperatures above 3000°F near the stagnation region at the nose. This temperature is above the single use limit of shuttle tiles and may lead to tile slumping. Based on the above validation exercise and other validation work related to the Space Shuttle,¹⁶ it is estimated that the predicted temperatures are accurate to within $\pm 25^\circ\text{R}$ over most regions of the vehicle.

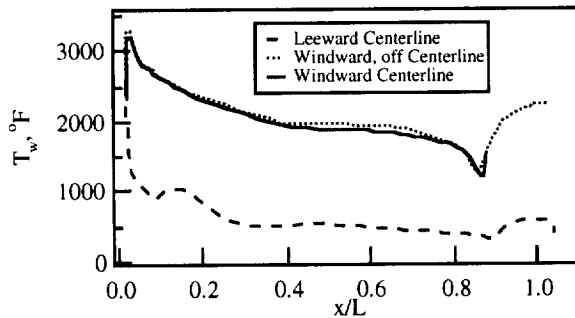


Fig. 9 Temperature vs. x/L , Mach 25.5 case.

The trajectory time discretization presented in Fig. 8 for the nominal flight trajectory is based on the discretization of the heating pulse experienced by the vehicle. Changes in the vehicle design resulted in modifications of the flight trajectory as well as shape changes. Therefore additional CFD simulations were required. The grid generation strategy outlined in the previous section allowed for quick grid modifications using OutBound and re-clustering to create a new grid.

X-33 GRID GENERATION STRATEGIES AND REFINEMENT STUDIES

The Reacting Flow Environments Branch at NASA-Ames has been involved with the X-33 program from the initial vehicle evaluation process, through the preliminary and critical design phases, to the final stages of the program. The X-33 program is a cooperative agreement between NASA and Lockheed-Martin Skunkworks to develop an experimental sub-orbital hypersonic flight test vehicle, the first flight of which is scheduled for 1999. This vehicle, a half-scale model of the commercial version of Lockheed-Martin's Reusable Launch Vehicle (RLV), represents the synthesis of a lifting body with innovative composite structures and cryotanks, a linear aerospike rocket engine, and a metallic Thermal Protection System (TPS).

If the vehicle performance is such that a single trajectory can be identified as the critical trajectory for the TPS design, then the environment can be obtained for the specific trajectory. If the vehicle design requires considerations from several trajectories, then the environment for each trajectory can be constructed and the worst case that affects the individual design decision can be assembled. If the trajectories are many, or as in the case of X-33, the design of the trajectory is coupled to the definition of the environment itself, then the trajectory-based approach becomes too expensive and does not provide the critical design focus in a timely manner. In response to the latter case, a new approach, called the Design Space Paradigm, was developed. CFD analyses of the X-33 configurations are carried out at several points on a trajectory and at points in a Design Space. For a given trajectory, a finite number of points are selected to obtain a good representation of the heat pulse while at the same time making sure the critical parameters of Mach number, angle of attack, and dynamic pressure (or Reynolds number) are covered. The Design Space computation involves the construction of a space parameterized by the same critical parameters encompassing most trajectories and permitting excursions at the lower dynamic pressure limit. The volume of the design space is discretized with sufficient denseness of points to assure that high-fidelity anchor points are available for the engineering method.

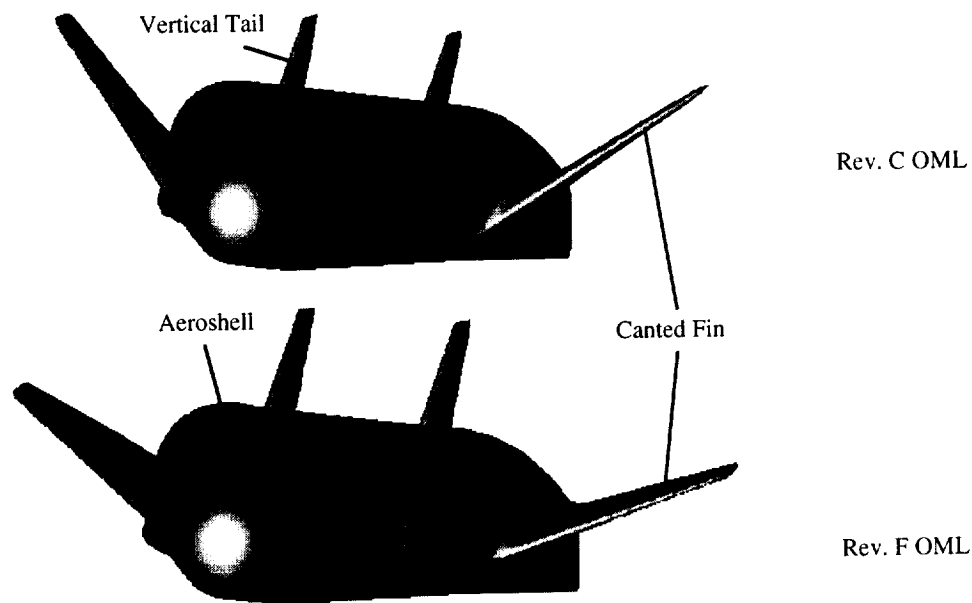


Fig. 10 Outer mold lines of the Rev.C and Rev.F "smooth" configurations considered in the aerothermal analysis of the X-33. The lower dihedral angle and larger vertical tails of the Rev.F geometry are clearly discernible. The aeroshell is the same for both configurations.

Vehicle Configurations

Three X-33 configurations have been: the D-Loft, Rev.C-Loft, and Rev.F-Loft configurations. The primary concern of this CFD work was the acreage aerothermal environments of the aeroshell, the canted fins, and the vertical tails only. As a result the body flap and engine ramp were not included in the numerical simulations nor in the grid generation process. Inclusion of these geometrical features would require consideration of the flow in the base region which creates an increased complexity in the grid generation process and a manifold increase in the computational requirements. Figure 10 shows perspective views of the Rev.C and Rev.F Lofts of the X-33 vehicle. The lower dihedral of the canted fins and larger vertical tails of the Rev.F-Loft are clearly seen.

Grid Generation Strategies

Generation of volume grids for the numerical calculations is the most important and time-consuming step in the aerothermal environment definition process and a great deal of care has to be exercised in the selection of the grid topology and placement of grid points to resolve key features of the flowfields. The grid generation process starts with the creation of a surface mesh from the definition of the Outer Mold Line (OML). Two approaches have been taken in the generation of the surface mesh. In the first approach, the CAD file obtained in (NASA)IGES format (translated from the original CATIA format) from Lockheed-Martin Skunkworks is processed in GridGen and a structured surface mesh of quadrilaterals (except at the nose tip singularity where the cells are triangles) is created. This approach is a very lengthy one requiring considerable amount of time to process the raw (NASA)IGES file to obtain the OML. In the second and shorter approach, the CATIA file is directly imported into HyperMesh and an unstructured triangulated surface is created. In either approach, the surface grid that is generated is verified against the original geometry and after certification by Lockheed Martin Skunkworks, a volume grid is generated.

For the D-Loft and Rev.C-Loft, the HypGen grid generation package was used to construct volume grids in a single-block topology. This hyperbolic grid-generation package starts with the surface mesh, a specified initial wall spacing, and surface orthogonality constraint of grid lines. It then creates layers of grids outward into the flowfield thus generating a volume grid. This is a trial-and-error process and requires several passes before a suitable volume grid is obtained. A difficulty of this single-block grid is the singularity at the nose tip which creates problems in the numerical integration of the flow equations. This volume grid, with a singularity at the nose tip, serves as the basis grid and several laminar perfect gas calculations (corresponding to various angles of attack and Mach numbers) are computed on this mesh. The code SAGE is then used to move the outer boundary closer to the outer bow shock and to re-cluster points near the wall. This process creates grids tailored to each angle of attack and Mach number of interest.

For the Rev.F-Loft, the commercial package, GridPro, was used to construct the volume grids. The triangulated surface mesh, obtained using HyperMesh (shown in Fig. 11), with a predefined outer surface (obtained from the earlier Rev.C studies) and an appropriate grid topology, were used to create multiblock volume grids which are then merged to yield a two-block inviscid volume grid.

The outer boundary derived from the previous Rev.C grid adaptations, was used to obtain a grid for each angle of attack. This eliminated the need to go through the additional steps of generating perfect gas flow fields and to use SAGE to move the outer boundary closer to the bow shock. A clustering algorithm in GridPro is then applied to the inviscid grid to add additional points in the shock layer to achieve the required clustering for viscous computations. A representative case of a volume grid generated using GridPro and the block topology implemented is shown in Fig. 12. A salient feature of a grid generated using GridPro is the nonsingular nature of the grid in the nose region. This is clearly seen in Fig. 13, which shows the nose region details of surface mesh of the Rev.C and Rev.F Lofts.

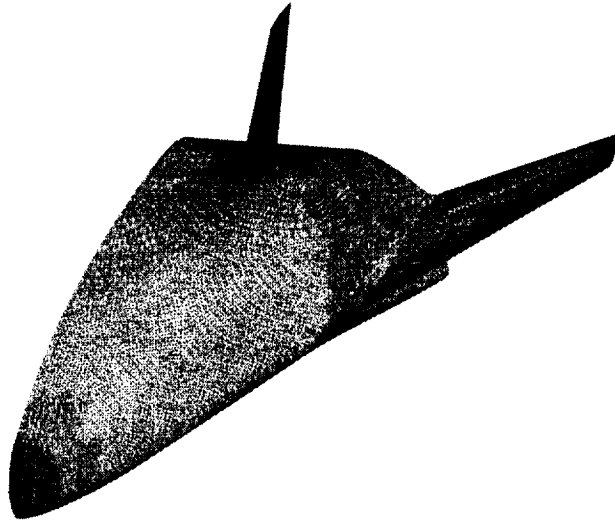


Fig. 11 Unstructured surface grid generated from a CATIA database using HyperMesh.

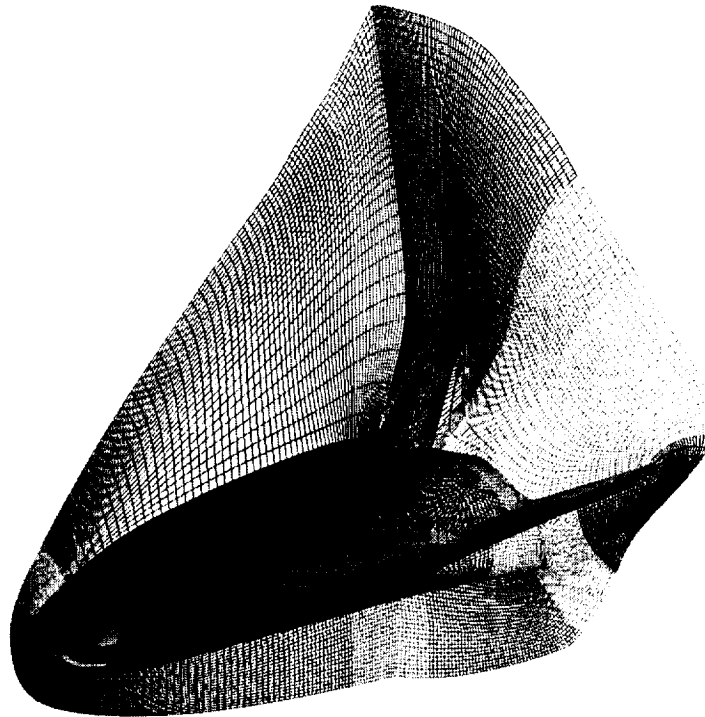


Fig. 12 X-33 block topology and volume grid generated for a 10° angle of attack case.

The most time consuming part of generating grids using GridPro is the time required to establish the initial grid topology. Once the grid topology is defined, grids for various angles of attack and Mach numbers can be generated more quickly (several days as compared to several weeks of the GridGen/HypGen approach).

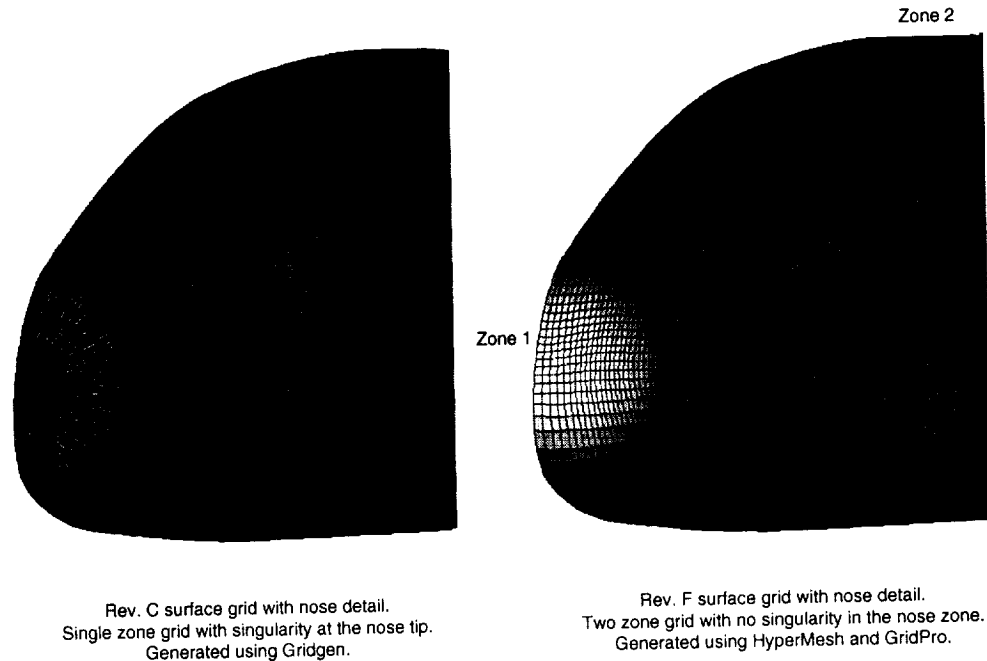


Fig. 13 Surface grids for the Rev.C and Rev.F configurations with details of the nose region.

Grid Sequencing Strategy

In order to speed up the convergence of the numerical integration process and also to establish grid-independence of the numerical solutions, a grid sequencing strategy is used. Starting with an initial grid that is four-times coarser than the final grid, converged solutions are obtained on grids of increasing fineness. The initial grid is four times coarser (in all directions) and the next grid is two times coarser (in all directions). These coarse grids are used to quickly establish the shock and the flow in the shock layer. The third grid in the sequence has full resolution in the normal direction and provides a reasonably accurate solution. The fourth grid in the sequence has full normal and circumferential resolution while being doubly coarse in the streamwise direction and this grid captures features such as the leading edge of the canted fin and the vertical tail to sufficient accuracy. Finally, the fifth grid in the sequence has complete resolution in all directions.

The peak laminar heating point on the X-33 Nominal Malmstrom-4 trajectory was chosen to establish the grid independence of the computed solution and the strategies required to achieve this independence. The Rev.C-Loft was chosen for this study the wall was assumed to be fully catalytic with a constant surface emissivity of 0.85. The solution is converged with a four to five-orders of magnitude reduction in the maximum residual for each grid in the sequence. However, the maximum residual is only one indicator of the convergence of the numerical solution. In addition, the surface quantities of interest such as the pressure and temperature are monitored at regular intervals. When the changes in these quantities are less than 0.5-1%, then convergence is assumed.

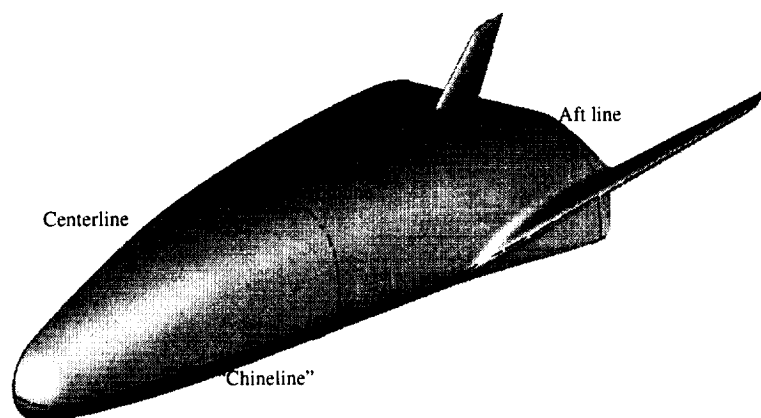


Fig. 14 Rev.C configuration with designated grid lines at which convergence is studied. The "chinline" passes along the leading edge of the canted fin, the midline is exclusively on the aeroshell, and the aftline passes through both the canted and vertical fins.

Figure 14 shows the Rev.C-Loft configuration with designated grids lines at which the pressure and temperature are compared for the three finest grids in the five-grid sequence. The computed surface pressures and radiative equilibrium surface temperatures for the three grids in the sequence are compared in Fig. 15 along the chinline. The greatest differences in the solutions occur between Sequence 3 and Sequence 2 grids and the differences are small between Sequence 2 and Sequence 1 grids. From this one can infer that for acreage calculations, Sequence 2 solutions are adequate. Having established the procedure for speeding up the convergence process and assuring grid independence of the solution, the same strategy is employed for all cases computed in the present work.

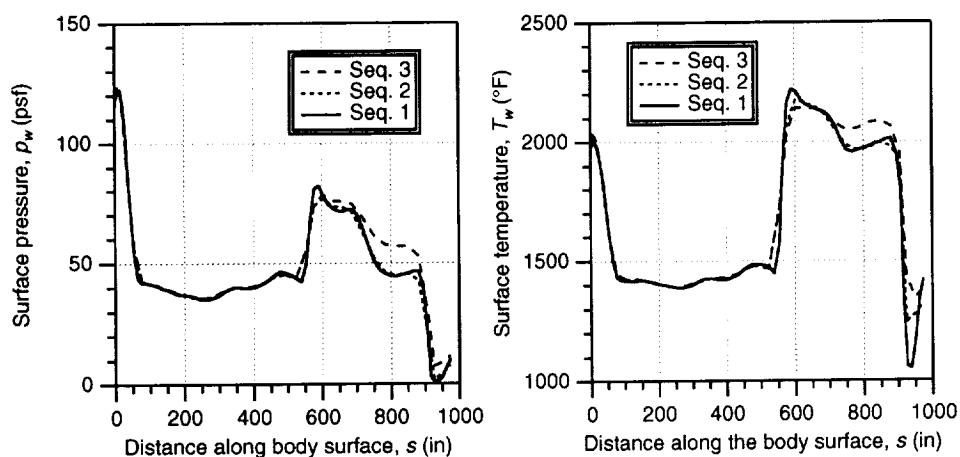


Fig. 15 Comparisons of the axial variation of surface pressure and temperature along the "chinline" for grids in Sequence 3,2, and 1. The "chinline" runs along the body chine and along the canted fin leading edge.

The differences between the radiative equilibrium temperatures from the Sequence 1 grid and the Sequence 3 grid (at corresponding locations) are depicted as isocontour plots in Fig. 16. It is clear from this figure that as far as acreage description of the environment is concerned, except for the leading edges of the fins, footprints of the shock-shock interaction, and the leeside vortices, the temperature differences are between $\pm 50^\circ\text{F}$. Thus, a Sequence 3 grid is sufficient to study trends very quickly and is economical from the point of view of computations.

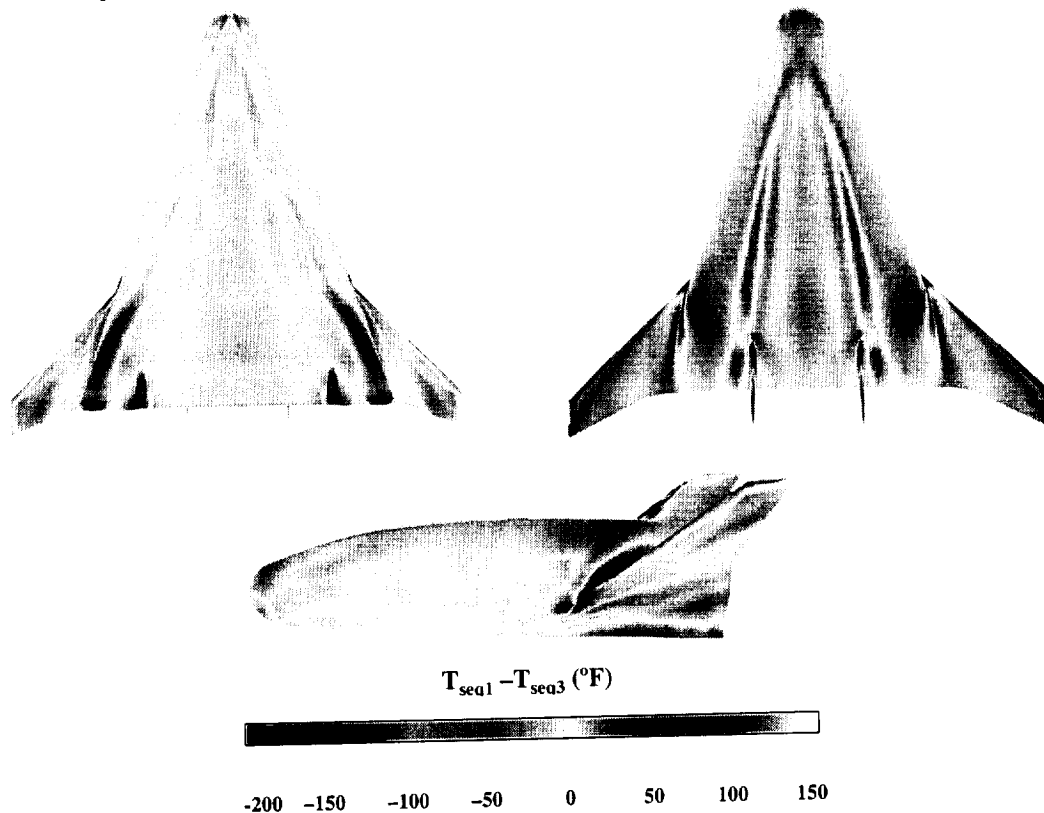


Fig. 16 Contours plots of the surface temperature difference between Sequence 1 (77x113x65) solution and Sequence 3 (39x57x65) solution for the Rev.C Loft at the peak laminar heating point ($t=352$ sec) on the Nominal Malmstrom-4 trajectory. The wall is fully catalytic with a constant surface emissivity of 0.85.

The X-33 work clearly established the viability of using CFD analyses in conjunction with engineering methods to create high-fidelity aerothermal databases for the design of the thermal protection system of the X-33. Such an approach would be extremely useful in the TPS design of the RLV and the TPS design of other hypersonic vehicles including planetary probes. The detailed results of the X-33 work are presented in Ref. 17.

Other important TPS design issues such as effects of yaw, topological constructs and computations of deflected control surfaces are presented as special topics. For the X-33 and the RLV configurations that have been analyzed, the simplified material map is fully catalytic with piecewise constant emissivities. The catalytic heating jumps across the material interfaces are purely due to emissivity changes. For an actual material map, the surface catalycity and emissivity are functions of surface temperature and these would have an impact on the surface temperatures and catalytic jumps across the material boundaries. Further, the surface grid definition at the material interfaces should be sufficiently fine to accurately capture the catalytic heating jumps. These issues are addressed in the forthcoming sections.

SPECIAL TOPIC - EFFECTS OF YAW

The splitlines for the nose region are determined using an aerothermal database with consideration of a $\pm 2^\circ$ sideslip. In all of the computations presented so far sideslip has been neglected and only one half of the vehicle has been considered with the pitch plane being treated as a computational boundary. The splitlines need to be assessed using CFD to provide anchor points for engineering. Toward this end, a sideslip of -2.5° is considered for the peak laminar and turbulent heating points on the Nominal Malmstrom-4 trajectory.

A complete three-dimensional grid is created by a simple reflection across the pitch plane and merging to obtain a two-zone grid with a nonsingular grid in the nose and a streamwise stack of O-grids for the remaining part of the body. The pitch plane on the leeside is the singular plane of the O-grid and is treated as a zonal boundary in the computations. In order to conserve time and quickly assess the impact of sideslip, the computations are limited to the Sequence 3 grid in the five-grid sequence, *i.e.*, the grid has full resolution in the normal direction but is two times coarser than the finest grid in the remaining two directions.

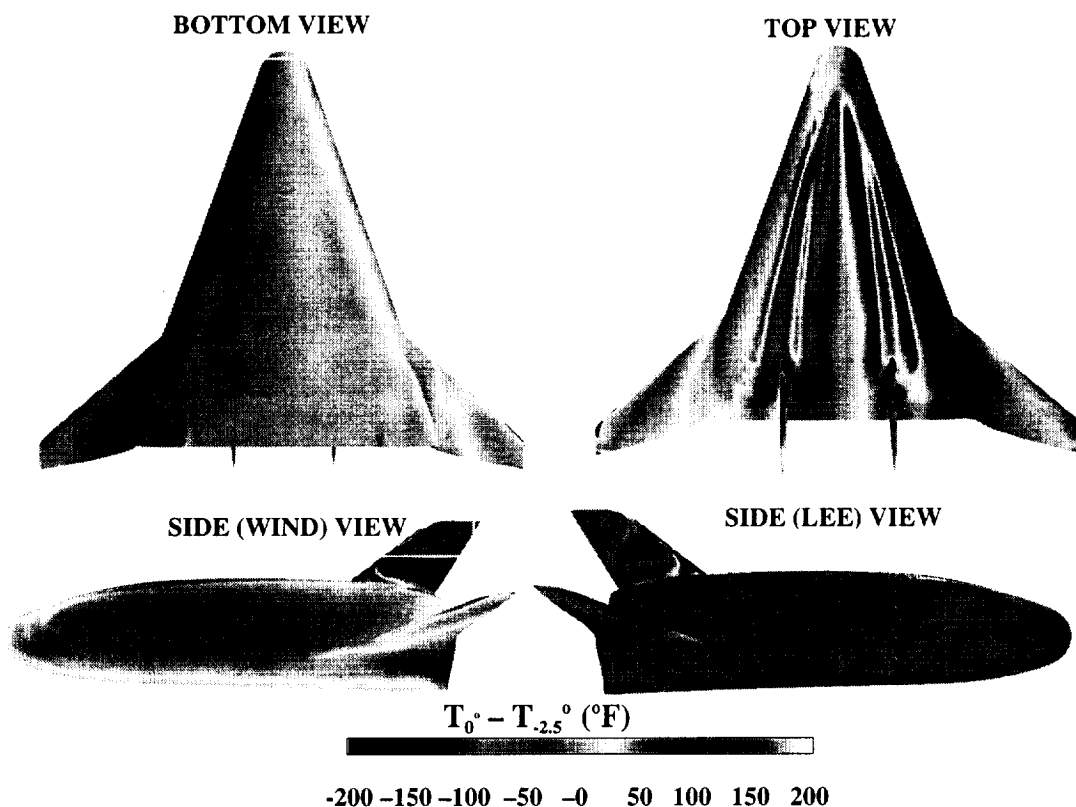


Fig. 17 Isocontours of the difference in computed radiative equilibrium surface temperatures for flow with and without yaw at the peak laminar heating point ($t = 352$ sec, $Ma = 11.44$, $\alpha = 35.8^\circ$, $Re = 46,232/\text{ft}$) on the Nominal Malmstrom-4 trajectory. The solutions are for the Rev.C Loft at yaw angles of 0° and -2.5° . The wall is assumed to be fully catalytic with emissivity of 0.85 for both cases.

The example presented here demonstrates the importance of grid refinement and the significance of grid quality to accurately capture complex physical phenomena. It would be interesting to compare two solutions (with and without yaw) in terms of the change in temperature at all points on the body surface. Such a comparison is presented here for the peak laminar heating point on the Nominal Malmstrom-4 trajectory. Figure 17 shows, in four views, isocontours of the surface temperature difference between the Sequence 3 grid solutions for the zero sideslip and -2.5° sideslip cases. The temperature differences are

about 50 °F over most of the body except for a small portion of the canted fin leading edge, the vertical fins, and the leeside where the differences are as high as 150 °F. The impact of sideslip on the vertical fin is quite significant and the interaction between sideslip and the leeside vortices is quite strong. The Sequence 3 grid is doubly coarse in the streamwise and the circumferential directions. From the grid convergence study, the differences in the Sequence 1 and Sequence 3 grids have been studied and quantified and thus the applicable decrements/increments are known approximately.

SPECIAL TOPIC - CONTROL SURFACES

The second special topic considered is the aerothermal environments for deflected control surfaces (rudders on the vertical tail and elevons on the canted fin) as shown in Fig. 18. In principle, the control surface deployment schedule can be considered within the Design Space parametric studies. To meet schedule and cost constraints, it would require an enormous amount of computer resources to generate aerothermal environments for several deflection settings of the control surfaces at each Design Space point. This approach is clearly not viable. A better alternative would be to consider the control surface deflections at "critical" points in the Design Space and use these high-fidelity computed aerothermal environments with simple theories and correlations along with the actual control surface deflection schedules to generate the approximate aerothermal environments.

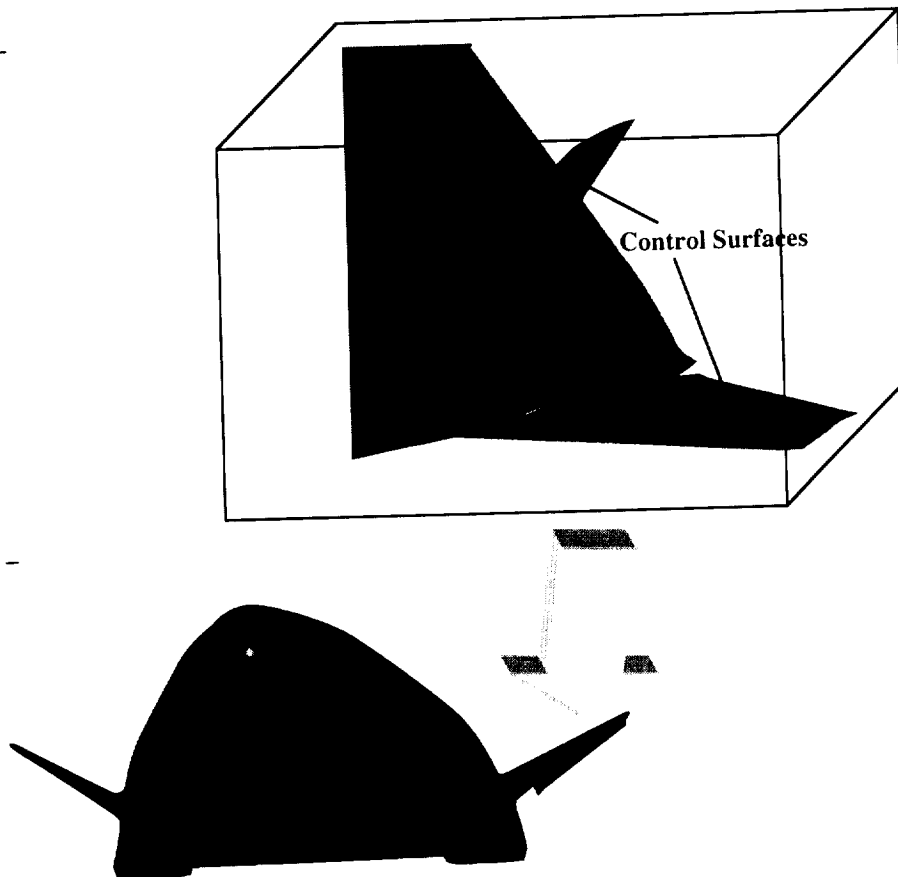


Fig. 18 X33 deflected control surfaces.

At the initial stages the maturity of the design details were not sufficient to model the gaps. For example the shapes of the static and moving parts, the gap width, both streamwise and axial, and the structural/mechanical elements were not defined at all, and a preliminary assessment was required. A simplified approach was adapted where no flow is assumed through the openings between the control

surfaces and the root region of a wing/fin. This assumption allowed the construction of a wrap around topology in this region, simply connected and mergable to the rest of the topology representing the vehicle geometry. Another approach also implemented was to build a grid around the control surface itself and to use chimera tools to interpolate the flow from the neighboring zones.

For the X33 analysis, control surface deflections were considered at Design Space points lying closest to the peak heating points on the design trajectories. In particular, control surface deflections of 10° and 25° were considered at $M=9$, $\alpha=20^\circ$, $Re=200,000/ft$ and $M=12$, $\alpha=35^\circ$, $Re=75,000/ft$ points in the Design Space. Solutions on the wrap around topology are presented in Fig. 19. The wrap around grid topology for each control surface setting is generated using a combination of Gridgen and HYPGEN. For simplicity, the gap between the deflected elevon and the canted fin (also the deflected rudder and vertical tail) is treated as a solid boundary (no flow through). The environments are computed for both laminar and turbulent flow conditions. Figure 19 shows the isocontours of the computed radiative equilibrium surface temperature for the windward face of the canted fin and the body chine for the 0° , 10° , and 25° outboard deflection cases. On the windward faces of the canted fin and elevon, it is clearly seen that the temperature increases with elevon deflection. This is due to flow compression by the deflected control surface. The influence of this compression on the body chine is negligible. The elevon (Rev. C)/(Rev. F) surface is assumed to be fully catalytic with an emissivity of 0.8. The same approach was adapted for the deflection studies of the rudder. It is emphasized here that these Design Space points, at which deflected control surface environments are computed, do not correspond to a specific trajectory and, as such, the high Reynolds numbers corresponding to these points would result in high temperatures.

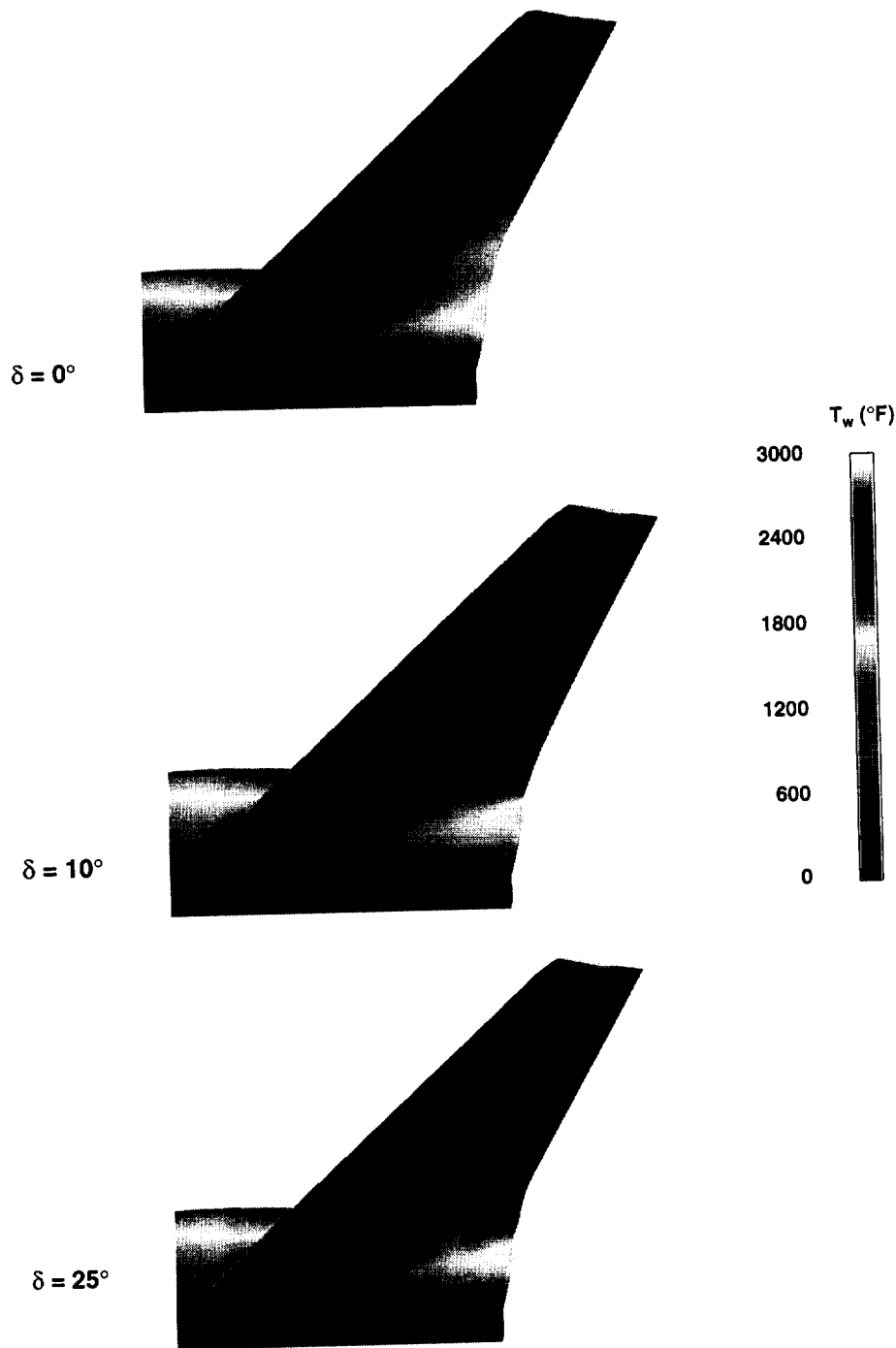


Fig. 19 Radiative equilibrium surface temperature contours for the outboard surface of the canted fin of the X-33 Rev. C configuration with 0° , 10° , and 25° elevon deflections (outboard). The computations are at a Design Space point at which $Ma=12.0$, $\alpha=35^\circ$, $Re=75,000/\text{ft}$. The temperature scale is the same for all three figures.

A number of alternate grid topologies were generated using GridPro for modeling the flow in and around deflected control surfaces. The approach taken here was to simplify the geometry around the edges by assuming no gap between the control surface and the main body along the hinge line. The area of concern

here is the gap between the deflected control surface and the main body at the root of the wing, fin or tail. Two general topological constructs were evaluated. An additional assumption is made for the first evaluated topology that there is a small vertical clearance on the sides of the control surface. This topology was found more difficult to construct and resulted in the clustering of a lot of points with highly skewed cells in the gap opening. The second topology assumed no gap on the sides of the control surface and provided a better strategy. The only implication is that the topological complexity needs to be carried in the normal direction all the way to the outer boundary. (The types of topologies evaluated here were not implemented for the X33 configuration mostly because of the increased topological complexity.)

GRID STRATEGIES FOR MODELING MATERIAL MAPS INCLUDING SPLIT LINES

The choice of grid topology and distribution of grid points is dictated by the primary objectives of the computations, required resolution of the flow features, and the physics of the flow. An example to illustrate the grid generation requirements for X-33 follows. The X-33 computations were performed with the primary aim of providing high-fidelity aerothermal environments for the design of the thermal protection system of the vehicle. The main assumption for the design computations is that the vehicle surface is fully catalytic, *i.e.*, the atomic oxygen and nitrogen species in the shock layer recombine completely at the wall to give molecular oxygen and nitrogen, respectively. The heat release due to recombination, in addition to the heating due to the wall-bounded shear flow, gives a "conservative" estimate of the heating to the vehicle surface. Tight integration of high-fidelity CFD techniques into the design cycle puts constraints on the turnaround time of the solutions. Under these constraints, a simple one- to two-block topology, with adequate number of grid points to resolve the dominant flow features, is chosen. The two-block topology, in particular, consists of a nonsingular block in the nose region. This considerably helps in obtaining solutions (at very low angles of attack) that are not contaminated by the singular axis. This global analysis for the X-33 vehicle, with approximately 500,000 to 750,000 grid points, has been successfully used for the design of the thermal protection system.¹⁷



Fig. 20 A perspective view and windside view of the nose region of the X-33 vehicle. The nose cap (dark region) is noncatalytic material and the remainder of the body surface is catalytic material. For both materials the emissivity is assumed to be 0.8

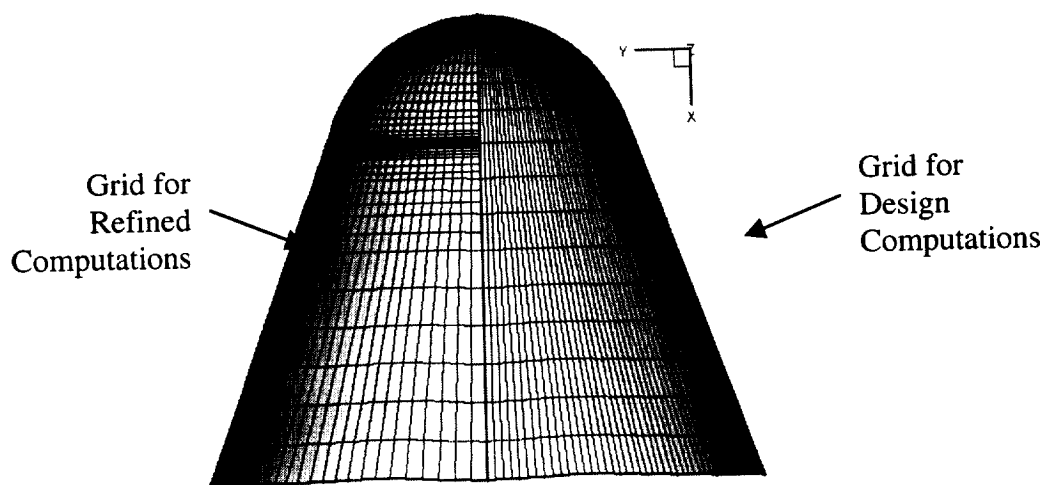


Fig. 21 Windside view of the surface grids used in refined analysis (left) and design computations (right). Note the streamwise clustering of points at the material interface. Both grids are based on a single-block topology with a singularity at the nose tip.

The design analysis has to be refined for pre-flight predictions. The refinement involves the inclusion of surface catalysis of actual materials/coatings along with grid refinements, *i.e.*, the design assumption of a fully catalytic surface is relaxed and finer grids are used. As a first step in this direction, the actual materials map is simplified to two materials - one in the nose-cap (either catalytic, non-catalytic, or partially catalytic) and one for the remainder of the aeroshell (either catalytic, non-catalytic, or partially catalytic). The lead manufacturing time for Carbon-Carbon nose cap is around 12-18 months. As a result of this requirement, the nose-cap aeroshell interface problem has a significant programmatic impact. To help this and as well as to assess the decisions made early in the project design cycle, the current study was undertaken. Two views of this map are shown in Fig. 20. Various possible combinations of material types are considered in the computations. For all the materials, the surface emissivity is assumed to be 0.8 independent of surface temperature. Fig. 21 shows the wind-side view of the surface grids used in the design computations ($M_\infty=11.44$, $\theta=35.8^\circ$, $Re=46232/ft$) and in the refined analysis. The grid refinement at the material interface (see Fig. 20) more accurately captures the "jump" in temperature across it. This jump will occur because the excess atomic species available on the nose-cap (due to the non-catalytic wall assumption) will have to recombine on the aeroshell (due to the fully catalytic assumption). Fig. 22, which shows the streamwise distribution of the computed radiative equilibrium surface temperature on the windward centerline, clearly brings out the effect of grid refinement in accurately capturing the temperature jump at the interface. Grid refinement studies were performed for various spacings at the material interface.¹⁸ Fig. 23 shows the comparison of radiative equilibrium surface temperature contours between the partially catalytic case and the design case at the same conditions. It is evident that the temperatures are much reduced in the nose-cap region because the material considered is relatively non-catalytic. The local increase in temperature at the material interface is also seen. There is significant increase in temperature beyond that used in the design of the thermal protection system and this increase must be accounted for in a conservative design.

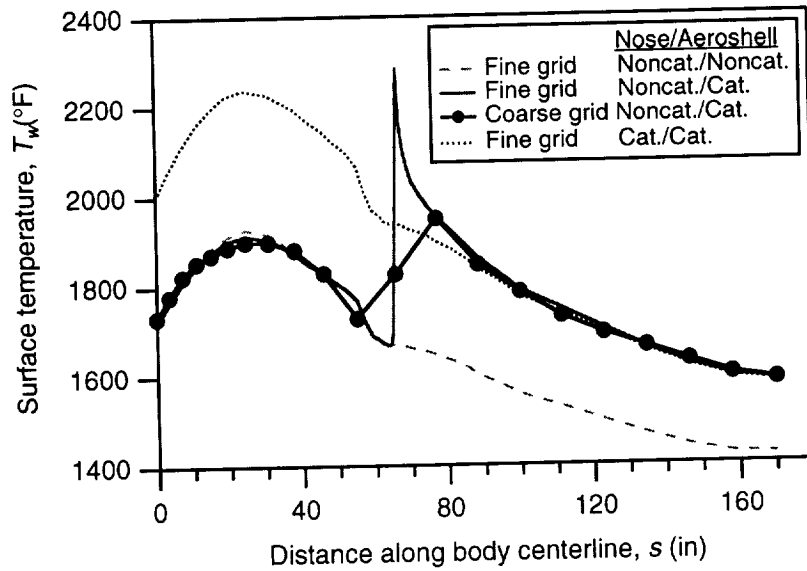


Fig. 22 Comparison of computed radiative equilibrium surface temperatures along the windward centerline for the design and refined grids. The nosecap is assumed to be noncatalytic and the remainder of the body is assumed to be fully catalytic. The surface emissivity is assumed to be 0.8 for both regions. Also shown are the computed radiative equilibrium surface temperatures for a completely noncatalytic body and a fully catalytic body on the refined grid.

It must be noted here that the refinement considered in Ref. 18 does not extend all the way circumferentially on the body, *i.e.*, the refinement at the interface is confined to the windward centerline and a nearby region and no such refinement is done for the rest of the interface towards the leeside of the vehicle. This refinement is acceptable for high angles of attack. Strictly speaking, to cover the entire angle of attack range, one should have complete resolution of the material interface. While this seems quite simple for the body considered, the topology can get extremely complicated for the entire vehicle which has several areas of dissimilar materials. Resolution of the catalytic jumps at all the interfaces will require multi-block topology.

NOSE - COATING A
AEROSHELL - COATING B

NOSE - CATALYTIC
AEROSHELL - CATALYTIC

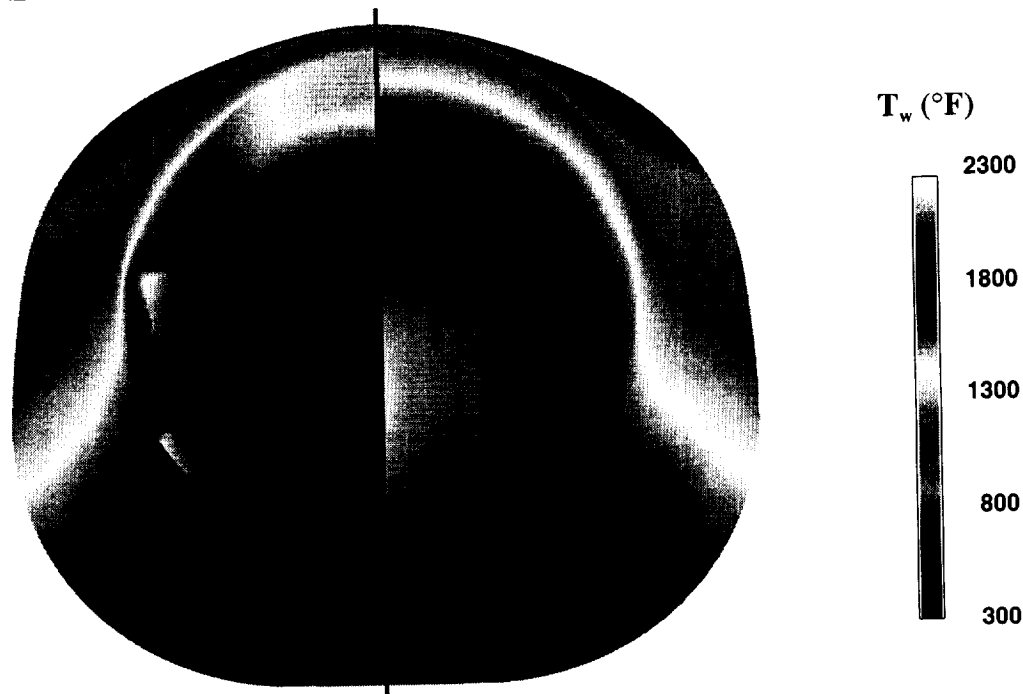


Fig. 23 Contours of computed radiative equilibrium surface temperatures in the nose region. The contours on the right correspond to the design case (fully catalytic wall) and the contours on the left correspond to the refined case (Coating A for the nosecap and Coating B for the aeroshell).

FUTURE CHALLENGES

This paper has described efficient grid generation strategies for obtaining high-fidelity CFD solutions for both global and detailed vehicle design problems; the acreage heating predictions to generate TPS split lines and the deflected control surface analysis are respective examples of these design problems. In the past, high-fidelity CFD has been applied sparingly to the analysis of global and detailed vehicle design problems because of both high costs and long run times. In X-33, and X-38, CFD has become a common element and a major driver in the design process. Three challenges of the future relating to CFD and grid generation are: 1) to provide designers with sensitivity information relating to various design changes, 2) to move high-fidelity information earlier into the design process, and 3) to smoothly integrate information from various disciplines. The impact of these challenges on grid generation are discussed in the following paragraphs.

In the vehicle design process, to make better decisions, engineers desire sensitivity information regarding the relationship between system, subsystem, or mission configuration changes and the new performance of the affected vehicle components. One strategy for quickly generating sensitivity information is to convert serial processes to parallel ones by generating large databases. For example, on X-33, trajectory information needed for performing the acreage TPS analysis was converted to a parallel process by generating a large CFD database that spanned the expected trajectory envelope. For a specified trajectory, TPS performance is predicted by interpolating within the database of CFD anchor points. Thus, once the CFD database is generated, a TPS analysis can be quickly performed for any trajectory. Therefore, sensitivity information regarding trajectory changes on the TPS performance is quickly provided to the designer. The advantage of this approach is that all the CFD solutions can be generated in parallel once the trajectory space is defined and discretized. The disadvantage of this approach is that many more CFD

solutions are generated than are necessarily needed. For example, on X-33, a database typically consists of 100 CFD solutions. In the future to accommodate more sensitivity parameters, it is expected that database sizes will grow to encompass 10,000 CFD solutions or more.

CFD databases of 10,000 CFD solutions necessitate a number of grid generation requirements. First, the time spent on generating each grid must be minimal and the process must be automated as much as possible. Second, metrics regarding grid quality for a given application are needed; for example, a cell Reynolds number (see Eq. 1) is a grid quality metric for a CFD heating calculation. Grid metrics are beneficial for automating the grid generation process and for certifying the quality of a CFD solution on a given grid.

Before a CFD solution can be used in a design database, the quality of the solution must be assessed; a large part of the assessment process involves distinguishing between actual flow features and errors in the flow solution resulting from inadequate grid resolution or an error in the grid. As the number of solutions increases, the time spent on quality assessment becomes large. Thus, grid metrics and grid standardization procedures are needed to reduce the time spent on solution quality assessment.

The second grid generation challenge involves moving high-fidelity results earlier into the design process. It is believed that increasing the fidelity of the early design process will lead to more accurate cost estimates and help identify potential design flaws; this area is a major thrust of IDS. For grid generation, the CAD to grid generation process can be very time consuming for complex geometries. For example, generating a surface grid for a detailed fighter aircraft is very labor intensive and can take as long as 6 months. Thus, to use CFD in preliminary design, the time and labor spent on the CAD to grid process must be significantly reduced.

Finally, as part of integrated vehicle design, information from one disciplinary analysis is usually needed for a number of analyses. Further, many of these problems are coupled. For example, on X-33, the coupled fluid-thermal analysis of panel bowing has been studied. This type of work requires grid compatibility between two disciplines that have different grid requirements. Developing the grid interfaces for the analysis can be very time consuming. Thus, simplified grid generation procedures for handling multi-disciplinary analyses are needed.

CONCLUSIONS

Recently, Computational Fluid Dynamics (CFD) codes and computer hardware advancements have evolved to a point where solutions of the full Navier-Stokes equations can be used in a timely and accurate manner in the vehicle design process for the prediction of trajectory-based aerothermal environments. Future grid generation codes need to be fast, robust, and highly automated to be integrated in system design and optimization cycles. New age space systems design requires continuous surface and volume grid modifications to reflect vehicle configuration changes ("diamorfining") resulting from design optimization.

Currently a typical design cycle includes a number of CFD solutions over a baseline vehicle configuration and a parametric investigation of important design parameters for aerodynamic and aerothermodynamic performance. Further determination of design sensitivities leads to perturbations and modification of the initial baseline vehicle configuration (outer mold line). A number of cycles may be necessary to complete a vehicle design. Current grid generation codes are highly interactive and labor intensive. To make grid modifications within a design cycle requires an efficient and highly automated grid generation capability.

It is also advantageous to make grid modifications within a single design cycle. For example, at hypersonic flow conditions a generic inviscid volume grid can be initially used to compute and estimate the outer flow boundary. The volume grid can then be regenerated, clustered to a viscous wall and adapted to regions of strong gradients. In addition, some design parameters are fairly well established after a small number of

flow iterations. Partially converged solutions can be used for incremental shape "diamorphing" and also to initialize the computational domain for the next design cycle, thus conserving the computational expense.

In addition, integrated design systems require multi-disciplinary optimization. This implies sharing of CAD data, surface and volume grids across platforms and applications, with different specific grid requirements. For automated design, future grid generation codes should be able to modify existing grids and CAD from other applications to the specific quality requirements for CFD use. Advanced grid expert systems should provide optimal topological constructs for a prescribed computational volume, and flow resolution requirements.

Finally some specific lessons learned with respect to grid generation and refinement for the accurate calculation of a vehicle's aerothermodynamic environment are summarized as follows:

- Grid refinement studies are recommended on simplified shapes first.
- Grid characteristics:

Wall spacing

- Heat transfer is very sensitive to normal grid spacing at the wall (vehicle surface)
- Wall Cell Reynolds no. $< 0.5 - 5$
- Wall spacing requirement can change as angle of attack changes

Topology

- Heat transfer seems insensitive to grid resolution at the shock, but shock alignment is necessary.
- Avoid singular lines in the boundary layer
- The capability to change number of points across boundaries is good for complex shapes

- Flow solver

- Changing limiter can change grid requirements
- Changing the Flux splitting algorithm can change the grid requirements
- When the streamwise grid resolution is coarse, a thin-layer approximation provides equally accurate solutions as a full viscous calculation
- For turbulent flow simulations, the wall spacing should be adequate to resolve the laminar sub-layer with a y^+ less than or equal to one

REFERENCES

- ¹ Pointwise, Inc., PO Box 210698, Bedford, TX 76095-7698, *Gridgen User Manual version 12*, 1997.
- ² Chan, W. M., Chiu, I.-T., and Buning, P. G., "User's Manual for the HypGen Hyperbolic Grid Generator and the HGUI Graphical User Interface," NASA, TM-108791, 1993.
- ³ Stager, J. L., and Rizk, Y. M., "Generation of Three-Dimensional Body-Fitted Coordinates Using Hyperbolic Partial Differential Equations," NASA, TM-86753, 1985.
- ⁴ Walatka, P. P., Buning, P. G., Pierce, L., Elson, P. A., "PLOT3D User's Manual," NASA, TM-101067, 1990.
- ⁵ Altair Computing, Inc., 1757 Maplelawn Drive, Troy, MI 48084, *HyperMesh 2.1 User's Manual*, 1997.

- ⁶ Program Development Corp., 300 Hamilton Avenue, Suite 409, White Plains, NY 10601, *GridPro/az300 - User's Guide and Reference Manual*, 1996.
- ⁷ Nakahashi, K., and Deiwert, G. S., "A Self-Adaptive-Grid Method with Application to Airfoil Flows," AIAA Paper 85-1525, July 1985.
- ⁸ Davies, C. B. and Venkatapathy, E., "The Multidimensional Self-Adaptive Grid Code SAGEv2," NASA, TM-110350, 1995.
- ⁹ Vinokur, M., "On One-Dimensional Stretching Functions for Finite-Difference Calculations," *Journal of Computational Physics*, Vol. 50, No. 2, May 1983.
- ¹⁰ Campbell, C. H., Caram, J., Berry, S., DiFulvio, M., and Horvath, T., "Overview of X-38 Hypersonic Wind Tunnel Data and Comparison with Numerical Results," AIAA Paper 97-0567.
- ¹¹ Campbell, C. H., Caram, J., Berry, S. and Horvath, T., "An Overview of XCRV Hypersonic Aerothermodynamic Wind Tunnel Data and Comparison With Numerical Results," AIAA Paper 97-2475.
- ¹² Berry, S. A., Horvath, T. J., Robach, V. E., and Williams, G. B. Jr., "Results of the .0362-Scale X-38 (Rev. 3.1) Vehicle Aerothermodynamic and Boundary Layer Transition Test in the NASA Langley 20-Inch Mach 6 Tunnel," NASA TM 112857, 1997.
- ¹³ Merski, N. R., "A Relative-Intensity Two-Color Phosphor Thermography System," NASA TM 104123, 1991.
- ¹⁴ Merski, N. R., "An Improved Two-Color Relative-Intensity Phosphor Thermography Method for Hypersonic Wind Tunnel Aeroheating Measurements," Ph.D. Dissertation, George Washington University, 1997.
- ¹⁵ Loomis, M. P., Venkatapathy, E., Papadopoulos, P., Davies, C. B., Berry, S., Horvath, T., and Cambell, C., "Aeroheating and Aerodynamic CFD Validation and Prediction for the X-38 Program," AIAA Paper 97-2478, Jun. 1997.
- ¹⁶ Olynick, D. R., and Tam, T., "Trajectory-Based Validation of the Shuttle Heating Environment," *Journal of Spacecraft and Rockets*, Vol. 34, No. 2, 1997.
- ¹⁷ Prabhu, D. K., Loomis, M. P., Venkatapathy, E., Polsky, S., Papadopoulos, P., Davies, C. B., Henline, W. D., "X-33 Aerothermal Environment Simulations and Aerothermodynamic Design," AIAA Paper 98-0868, 36th Aerospace Sciences Meeting, Reno, Nevada, January 1998.
- ¹⁸ Prabhu, D. K., Venkatapathy, E., Kontinos, D. A., and Papadopoulos, P., "X-33 Catalytic Heating," AIAA Paper No. 98-2844, 7th AIAA/ASME Joint Thermophysics and Heat Transfer Conference, Albuquerque, New Mexico, June 1998.

¹⁹ Olynick, D. R., "Importance of 3-D Grid Resolution and Structure for Calculating Reentry Heating Environments," AIAA 96-1857, June 1996.

²⁰ Olynick, D. R., and Henline, W. O., "Navier-Stokes Heating Calculations for Benchmark Thermal Protection System Sizing," Journal of Spacecraft and Rockets, Vol. 33, No. 6, pp. 807-814.